

Thermodynamics of Na_8 and Na_{20} clusters studied with *ab initio* electronic structure methods

Abhijat Vichare and D. G. Kanhere¹

Department of Physics, University of Pune, Ganeshkhind, Pune 411 007,
INDIA

S. A. Blundell²

Département de Recherche Fondamentale sur la Matière Condensée, CEA
Grenoble
17, rue des Martyrs, F-38054 Grenoble CEDEX 9, France

Abstract

We study the thermodynamics of Na_8 and Na_{20} clusters using multiple-histogram methods and an *ab initio* treatment of the valence electrons within density functional theory. We consider the influence of various electron kinetic-energy functionals and pseudopotentials on the canonical ionic specific heats. The results for all models we consider show qualitative similarities, but also significant temperature shifts from model to model of peaks and other features in the specific-heat curves. The use of phenomenological pseudopotentials shifts the melting peak substantially (~ 50 – 100 K) when compared to *ab initio* results. It is argued that the choice of a good pseudopotential and use of better electronic kinetic-energy functionals has the potential for performing large time scale and large sized thermodynamical simulations on clusters.

1 Introduction

The physics of finite-sized systems such as clusters continues to invoke considerable interest both in theory and experiment. A particularly intriguing and poorly understood phenomenon is the melting behavior of such finite-sized systems. Only recently have Haberland *et al.*[1] succeeded in measuring the

¹(amv, kanhere)@unipune.ernet.in

²sblundell@cea.fr

heat capacity of free (i.e. unsupported) Na_n^+ clusters, with n ranging from 70 to 200 atoms. Interestingly, they find a nonmonotonic behavior of the melting temperature as a function of cluster size, with pronounced maxima at $n = 57$ and 142. These sizes correspond neither to closed-shell Mackay icosahedra ($n = 55$ and 147) nor to closed shells of valence electrons ($n = 59$ and 139), but are intermediate between the two. This clearly indicates that both geometric and electronic shell effects contribute to the melting phenomenon in a rather subtle manner.

Prior to this measurement, there have been a few experimental studies on melting of clusters. Martin *et al.*[2] reported measurements on the melting temperature of Na clusters for the sizes of the order of thousands of atoms and their results indicated that the melting temperatures increased with size, but had not reached the experimental bulk value. Peters *et al.*[3] have noted the existence of surface melting on supported Pb nanoparticles using X-Ray diffraction.

Clearly, the melting behavior at small sizes is cluster specific and dependent on the nature of the electronic structure and geometry. Further, the transition found by Haberland *et al.*[1] is not sharp and has a broadened peak in the specific heat with a width of approximately 40 K. The expected monotonic increase of melting point has been seen only for very large clusters containing upwards of several thousand atoms. On the theoretical side, much insight into the finite-temperature properties has been gained via molecular dynamics (MD) and Monte-Carlo (MC) numerical simulations. Most of these simulations have been carried out using classical empirical two-body potential functions, [4] mostly of Lennard-Jones (LJ) or Morse type. These studies have revealed that small clusters exhibit a melting transition over a broad temperature range, unlike bulk systems, and have broad heat-capacity curves. In addition, they also exhibit a variety of other phenomena such as isomerization (including surface isomerization) and surface melting, which are generically referred to as “premelting” phenomena. Some clusters also exhibit coexistence of liquid-like and solid-like phases within the melting temperature range.

MD and MC simulations have also been reported using classical embedded-atom potentials, such as the single-moment approximation (SMA), [5, 6] which contain approximations to the N -body forces found in metallic sys-

tems like Na clusters. Calvo and Spiegelmann [7, 8] performed extensive simulations on Na clusters with from 8 to 147 atoms using the SMA potential of Li *et al.* [6] with a view to probe the melting phenomena of small Na clusters. They find that premelting phenomena dominate the melting process at small cluster sizes ($n < 75$), while the larger sizes exhibit a preference for a single-process melting. They also observe that the nature of the ground state is critical to the thermodynamics of the cluster. However, as they clearly point out, their simulations do not incorporate the electronic structure effects directly.

An alternative approach for metallic clusters is that of Poteau *et al.* [9, 10] who developed a tight-binding Hamiltonian to incorporate quantal effects approximately. They use a Hückel-type Hamiltonian and MC to sample the phase space for small Na clusters with 4, 8, and 20 atoms. Calvo and Spiegelmann [8] have performed more extensive calculations for sizes up to 147 atoms with the same potential. However, during the last decade developments in *ab initio* methods have opened up practical possibilities of performing accurate simulations by combining density functional theory (DFT) with classical MD or MC. The most accurate form of DFT is the Kohn-Sham (KS) formulation. Although these methods have been used to investigate the structural properties with remarkable success, relatively few applications of such *ab initio* methods have been to the simulation of melting. Jellinek *et al.*[11] have, however, combined a hybrid Hartree-Fock/DFT method with MC sampling to study the thermodynamics of Li_8 .

Although it is most desirable to have a full quantum mechanical treatment of electrons, as in the KS method, such simulations turn out to be expensive. It is also to be noted that typical simulation times used in purely empirical potential MD are of the order of a few 100 ps or more per energy point. Considering that the most relevant sizes for the experiment are in excess of 50 atoms, the full *ab initio* simulation may turn out to be practically too expensive.[12] Hence approximate methods leading to practical and fast algorithms have been developed. One such technique is density-based (DB) molecular dynamics, where the electronic kinetic energy is approximated as a functional of density only. For example, Vichare and Kanhere [13] performed *ab initio* simulations on an Al_{13} cluster to investigate its melting behavior. The DB method has also been used by Aguado *et al.*[14, 15] to study the melting of Na clusters ranging in size from 8 to 142 atoms. Their simulations

are of constant total energy type using empirical pseudopotentials with up to 50 ps of observation time per energy point for small clusters (8 and 20 atoms), and up to 18 ps per energy point for larger ones. Another approach is that of Blaise *et al.* [16] who carried out DB simulations for Na clusters up to size 274, but using soft, phenomenological pseudopotentials rather than *ab initio* pseudopotentials. In addition to permitting significantly longer observation times, these soft pseudopotentials were shown to reproduce well properties such as the volume and surface energies, ionization energies, and the frequency of collective ionic monopole and quadrupole oscillations.

These above-mentioned studies on Na clusters bring out a number of issues which need further investigation. Clearly, it is desirable to have both long simulation times and a full quantum mechanical treatment of electrons. Full KS being expensive, however, the attractive propositions of DB or soft pseudopotentials as practical alternatives for the simulation of such systems need to be assessed as to their quality. This is particularly important because of some discrepancies seen in the above studies. For example, in the case of Na₈, Calvo and Spiegelmann, [7, 8] using an SMA potential, find that the canonical specific heat is broad in nature and shows a flattened peak between about 110 K to 250 K. For the same cluster, the tight-binding potential [8, 9] leads to a less broad peak, with a width of about 70 K and peaking at 160 K. However, the microcanonical specific heat obtained by Aguado *et al.* [14] for Na₈ in a constant-energy DB study shows a peak at a much lower value of 110 K and is sharp with a width of less than 30 K. This is in qualitative disagreement with the SMA and tight-binding results.

Further, there is a difference in the way the data has been analyzed by these workers. Aguado *et al.* [14, 15] have used the traditional trajectory-based analysis, which uses the caloric curve supplemented by Lindemann type criteria for identifying the transition. Since the transition is never sharp, such an analysis may not lead to an unambiguous determination of the melting temperature. In addition, the observation times of Aguado *et al.* are significantly less than those used by Calvo and Spiegelmann [7, 8] in their SMA or tight-binding work. In fact, it is desirable to calculate appropriate thermodynamic indicators such as the ionic entropy and the specific heat. In Refs. [7, 8, 9], the authors have used the multiple histogram (MH) technique [17, 18] to extract the entropy and the specific heat from the simulation data, as we do here.

In the present work, we therefore examine the melting of Na_8 and Na_{20} clusters with a view to resolving these issues. We have carried out the following simulations on Na_8 : a full KS (orbital-based) simulation using *ab initio* pseudopotentials; a DB simulation, where the electronic kinetic energy is approximated, but with identical pseudopotential and time scales; and both KS and DB simulations with soft pseudopotentials. The same simulations have been carried out for Na_{20} , with the exception of the full KS simulation with *ab initio* pseudopotentials. In all the cases we have calculated the entropy and the canonical specific heat via the MH method, as well as the traditional indicators like the RMS bond length fluctuation and mean squared displacements.

In the next section, we briefly describe the formalism, analysis methods, and numerical details. In Section 3, we present our results and discuss them in the light of earlier studies. Finally, our conclusions are presented in Section 4.

2 Method

Following the usual procedure in DFT,[19] we write the total energy of a system of N_a stationary Na^+ ions with coordinates $R \equiv \{\mathbf{R}_i\}$ and N_e valence electrons as a functional of the electron density $\rho \equiv \rho(\mathbf{r})$

$$E_{\text{pot}}[\rho, R] = T[\rho] + E_{\text{ext}}[\rho, R] + E_H[\rho] + E_{xc}[\rho] + E_{ii}[R], \quad (1)$$

where $T[\rho]$ and $E_H[\rho]$ are the kinetic and Hartree energy, respectively, of the valence electrons, $E_{\text{ext}}[\rho, R]$ is the interaction energy of the valence electrons with the ions, evaluated using the pseudopotential formalism, $E_{xc}[\rho]$ is the electron exchange-correlation energy in the local density approximation (using the parametrization of Perdew and Zunger[20]), and $E_{ii}[R]$ is the ion-ion interaction energy. In the standard KS approach, $T[\rho]$ is expressed as a sum of expectation values, over each KS orbital, of the electron kinetic-energy operator $-(1/2)\nabla^2$. In contrast, in the DB approach $T[\rho]$ is expressed as a functional of ρ only, without introducing orbitals, leading to a faster though in practice less accurate calculational scheme. For each approach we use either *ab initio* (AI) pseudopotentials or soft, phenomenological (SP) pseudopotentials. We consider two forms for $T[\rho]$ in the DB approach: in our DB-AI

approach we use a functional form proposed for clusters,[21, 22] while in our DB-SP approach we take $T[\rho]$ as a sum of the Thomas-Fermi energy and a scaled Weizsäcker term. [16]

The *ab initio* pseudopotentials used in the KS-AI and DB-AI approaches are those proposed by Bachelet, Hamann and Schlüter.[23] The soft, phenomenological pseudopotential used in the KS-SP and DB-SP approaches is given by [16]

$$V_{\text{soft}}(r) = \begin{cases} -\frac{1}{r}, & r > r_c \\ -\frac{1}{6r_c} \left[7 - \left(\frac{r}{r_c} \right)^6 \right], & r \leq r_c, \end{cases} \quad (2)$$

for a single Na^+ ion at the origin, where $r_c = 3.55a_0$ in the DB-SP approach and $r_c = 3.7a_0$ in the KS-SP approach. The choice of r_c for the DB-SP approach follows from a fit to volume and surface energies,[16] while for the KS-SP approach the choice of r_c ensures close agreement with ionization energies and dissociation energies given by an *ab initio* pseudopotential, for small clusters in the size range $n = 3$ to 8. Use of the phenomenological pseudopotential permits a larger grid step size or equivalently a smaller plane-wave energy cut-off, thus leading to a faster solution in either the KS or DB formalisms. The Car-Parinello (CP) algorithm [24] was used in the DB-AI and DB-SP schemes, while the damping scheme proposed by Joanopoulous *et al.* [25] was used to minimise the electronic degrees of freedom in KS-AI.

The trajectories collected were analyzed using traditional indicators of melting like the rms bond-length fluctuation, defined as

$$\delta_{\text{rms}} = \frac{2}{N_a(N_a - 1)} \sum_{i < j} \frac{\left(\langle r_{ij}^2 \rangle_t - \langle r_{ij} \rangle_t^2 \right)^{\frac{1}{2}}}{\langle r_{ij} \rangle_t}, \quad (3)$$

where r_{ij} is the distance between ions i and j , and $\langle \dots \rangle_t$ denotes a time average. According to the Lindemann criterion, a system may no longer be considered to be solid if δ_{rms} is greater than 0.1 to 0.15. Short time averages over the trajectory data, e.g. over data points corresponding to 1 ps, 2 ps, 5 ps, etc., were evaluated to obtain the dependence of δ_{rms} on the duration of the time average. Another indicator we have used is the mean square ionic displacement, defined as

$$\langle \mathbf{r}^2(t) \rangle = \frac{1}{Nn_t} \sum_{m=1}^{n_t} \sum_{i=1}^{N_a} [\mathbf{r}_i(t_{0m} + t) - \mathbf{r}_i(t_{0m})]^2. \quad (4)$$

We have set the total number of time-steps n_t used in the time average to $n_t = n_T/2$, where n_T is the total simulation time (usually about 50 ps).

A more complete thermodynamic analysis of the simulations is possible using the multiple histogram method (MH), [17, 18] and all simulations were analysed using this method. It requires the configurational energy, which corresponds here to the classical potential energy $E_{\text{pot}}[\rho, R]$ of Eq. (1), over various points in the ionic phase space accessed by the system along the trajectory. This is used to evaluate the classical ionic density of states $\Omega(E)$, and thereby the ionic entropy $S(E) = \ln \Omega(E)$, as well as the partition function via a least-squares fitting procedure. The sampled values of the configurational energy are fitted to the theoretical probability distribution and the fitted coefficients are then used to evaluate the various thermodynamic functions. We consider in particular the canonical specific heat, defined as usual by

$$C = \frac{\partial U}{\partial T}, \quad (5)$$

where $U = \langle E_{\text{pot}} + E_{\text{kin}} \rangle_T$ is the average total internal energy in a canonical ensemble at temperature T . We here exclude the contribution of the center-of-mass motion to the ion kinetic energy E_{kin} , so that from the equipartition theorem

$$\langle E_{\text{kin}} \rangle_T = \frac{3}{2}(N_a - 1)k_B T. \quad (6)$$

The canonical probability distribution for observing a total energy E at temperature T is given by the usual Gibbs distribution

$$p(E, T) = \frac{1}{Z(T)} \Omega(E) \exp\left(-\frac{E}{k_B T}\right), \quad (7)$$

with $\Omega(E)$ the classical density of states extracted from the MH fit, and $Z(T)$ the normalizing canonical partition function. Note that although here we shall discuss results in the canonical ensemble, once $\Omega(E)$ is known, one may also evaluate properties in the microcanonical ensemble, such as the microcanonical temperature $T(E)$

$$\frac{1}{T(E)} = \frac{\partial}{\partial E} \ln \Omega(E). \quad (8)$$

Simulated annealing was used to obtain the ground-state ionic structures from a randomly chosen initial configuration for each cluster. For Na_8 the

ground-state geometry is found to have a dodecahedral D_{2d} symmetry in both the KS and DB formalisms and for both the AI and SP pseudopotentials, in agreement with the structure found by R  thlisberger and Andreoni [26] in a KS approach. For Na_{20} in the DB formalism, we find a ground state consisting of a double icosahedron with a single cap on its waist, which is the second of the two structures found in Ref. [26]. In the KS formalism, the ground state for Na_{20} is a double icosahedron missing one end cap and with two caps on the waist, in agreement with Ref. [26]. Our DB structures agree with those found by Aguado *et. al.*[14]

We have considered two approaches to the statistical sampling of the ionic phase space, required as input to the MH analysis. In each approach the clusters are effectively heated slowly from the ground-state structure at 0 K to a liquid-like state at upwards of 250 K. The first approach involves a canonical sampling of the phase space and was used with the AI pseudopotentials in both the KS and DB schemes. Successive simulation temperatures of 60 K, 80 K, 100 K, 125 K, 150 K, 175 K, 200 K, 225 K, and 250 K were chosen. Each temperature was maintained within ± 10 K using velocity scaling,[30] except for the 60 K and 80 K temperatures, where the temperatures were maintained within ± 5 K. The total observation time for both KS and DB is about 57.5 ps per temperature point. The initial condition at each temperature was taken as the final state of the previous temperature, and the initial 1.25 ps of simulation time were used to raise the previous temperature. The next 5 ps were then discarded to allow for thermalization of the system at the new temperature. The analysis was performed on the data corresponding to the last ~ 50 ps. The simulations for the clusters Na_8 and Na_{20} were performed within a cubical supercell of edge 40 a.u. [27] or more. All Fourier space evaluations were carried out on a mesh of $64 \times 64 \times 64$ for DB and $48 \times 48 \times 48$ for KS with a cutoff of about 21 Ry. The configuration energy range was divided into bins whose width was chosen to give at least about 30 points for the lowest temperature distribution. About 500 bins were typically used to cover the entire configuration energy range. The canonical specific heats obtained using the MH analysis were then plotted as a multiple of their value C_0 at 0 K given by $C_0 = (3N_a - 9/2)k_B$, which is the zero-temperature classical limit of the rotational plus vibrational specific heats.

Our second approach consists of a microcanonical sampling of the phase space, and was used with the SP pseudopotential in both the KS and DB

schemes. Constant total energy simulations were performed at closely spaced values of the total energy, such as to give good overlap of successive histograms of the potential energy E_{pot} . The simulations were performed in order of increasing total energy, with the initial condition at one energy obtained by scaling the velocities of the final state of the previous energy, and 20–30 energy points were used to scan the required energy range. Each energy point consisted of from 50–100 ps of observation time, of which 5–10 ps were discarded for equilibration. Several scans of the entire energy range were made in this way, giving *total* simulation times of about 15 ns for (Na_8 , DB-SP), 5 ns for (Na_8 , KS-SP), 6 ns for (Na_{20} , DB-SP), and 3 ns for (Na_{20} , KS-SP). The microcanonical sampling requires a modified MH analysis.[28] Note that DB-SP results have been reported elsewhere,[29] and are reproduced here for purposes of comparison.

The dominant error in our specific-heat curves is statistical, due to the finite duration of the sampling of the phase space. By adding extra data points, or complete additional scans of the whole temperature range, to the MH analysis, we find the specific-heat curves to be stable to about 10% or better, and the positions of peaks to be stable to about ± 20 K or better. We take this as an informal estimate of the statistical error. However, in dynamical simulations such as these, it may be that some processes of importance (e.g. isomerizations) occur on a physical time scale rather longer than we have considered, so that we have imperfect ergodicity; all we can say is that our curves do appear to be rather stable on the time scales that we have considered. We are currently considering recent Monte-Carlo sampling methods such as the parallel tempering method,[31] which are designed to overcome the problem of long time scales and improve ergodicity.

3 Results

We begin the discussion by considering some of the conventional trajectory-based indicators of isomerization and melting. In Fig. 1, we show the rms bond-length fluctuations δ_{rms} of Na_8 in the KS-AI model as a function of simulation time, for different temperatures in the range 60 K to 250 K. The figure makes it clear that for temperatures up to about $T = 200$ K, 25 ps

are sufficient to converge the value of δ_{rms} , while for higher temperatures of the order of 250 K or more, even longer simulation times may be required. Similar behaviour is seen in Fig. 2 for the 20-atom cluster simulated within the DB-AI model. In Fig. 3, we show δ_{rms} averaged over 37.5 ps and over 5 ps, as a function of temperature. Note that the 5 ps curve never crosses the Lindemann criterion of 0.1, while the 37.5 ps curve crosses the Lindemann criterion of 0.1 around 190 K. The behavior of δ_{rms} in DB-AI over identical simulation times is very similar.

The mean square ionic displacement $\langle \mathbf{r}^2(t) \rangle$ (4) has also often been used as an indicator of isomerization or of a solid-like to liquid-like transition. In Figs. 4 and 5 we show $\langle \mathbf{r}^2(t) \rangle$ on different time scales of 1 ps and 25 ps, respectively, for Na_8 in the KS-AI model. One observes that $\langle \mathbf{r}^2(t) \rangle$ at low temperatures $T < 100$ K reaches a horizontal plateau for $t > \sim 0.25$ ps, indicative of a solid-like behavior in which atoms vibrate around fixed points with an amplitude squared that increases in rough proportion to the temperature. On the other hand, the rising curve for $T \geq 250$ K suggests a liquid-like behavior with diffusion throughout the entire volume of the cluster. The curve for $T \geq 250$ K would eventually reach a plateau with a $\langle \mathbf{r}^2(t) \rangle$ value characteristic of the square of the linear dimension of the cluster, but even at $t = 25$ ps this plateau has not yet been attained. Somewhere between these two limiting temperatures is a region of isomerization processes with a character intermediate, in some sense, between solid and liquid.

The MH analysis may be used to probe further the thermodynamics of the cluster in any particular model. One here extracts the ionic entropy $S(E) = \ln \Omega(E)$, which is a functional of the potential-energy surface (1). As expected, all entropy curves show a monotonic increase, the curve for KS-AI, shown in Fig. 6, being typical. The canonical specific heats (5) for Na_8 obtained via the MH technique for all four models are shown in Figs. 7–10. In general, all the Na_8 specific-heat curves show broad peaks with widths over 100 K. The initial rise is around 70 K for both DB models. In the KS models, the initial rise of the main peak for the SP pseudopotential is at a higher temperature than for the AI pseudopotential, namely, at 200 K compared to 150 K. However, the KS-SP model has a shoulder feature around 80 K not visible in the KS-AI results. Turning to Na_{20} in Figs. 11–13, we find main peaks that are less broad than for Na_8 , with a width generally somewhat less than 100 K. In the DB models, the main peak for the AI pseudopotential is

at a higher temperature than for the SP pseudopotential, namely, at about 250 K compared to about 150 K. If on the other hand we compare the KS-SP model with the DB-SP model, we find that both main peaks occur at about the same temperature. However, the KS-SP model has a “premelting” feature around 80 K that is more distinct than for DB-SP model.

It is difficult to draw simple, general conclusions from these observations concerning the effect of the KS approach versus the DB approach, or the effect of AI versus SP pseudopotentials. For example, for Na_8 in the KS model, the SP pseudopotential gives a main peak at higher a temperature than for the AI pseudopotential (if one ignores the small premelting feature in the former), while for Na_{20} in the DB model, it is the AI pseudopotential that gives a peak at the higher temperature. For these small cluster sizes, the precise form of the specific-heat curves can evidently be very sensitive to the model used. One observes a similarly large variation in specific-heat curves between the SMA and TB models reported in Ref. [8]. Evidently, the important features of the potential-energy landscape can be rather sensitive to the model employed.

Some insight into the model-dependence of the potential-energy surface may be gained from the energetic ordering of a selection of possible isomers of Na_8 . We consider the dodecahedron D_{2d} (the ground state in all DB and KS models of this work, as well as in the SMA model [7]), the capped pentagonal bipyramid C_s (the ground state for LJ₈), and the stellated tetrahedron T_d . In the DB models and the SMA model, the C_s structure forms a relatively low-lying excited isomer at 0.03–0.05 eV above the D_{2d} ground state, while in our KS models and in the KS approach of Ref. [26], the C_s structure is unstable and collapses to D_{2d} upon relaxation. On the other hand, the T_d structure forms a higher-lying isomer at around 0.09–0.12 eV in the present DB and KS models, in the KS approach of Ref. [26], and in the SMA model, while in the TB model [8] and in an all-electron configuration-interaction approach,[32] the T_d structure is the ground state. This illustrates how even for Na_8 the ordering of isomers given by *ab initio* calculations is uncertain. We note that, while the heights of the barriers separating isomers are a more important determining factor than the simple energy differences, the existence of the low-lying C_s isomer in the DB models, but not in the KS models, is consistent with the lower-temperature shoulder of the Na_8 specific heat curve in the DB models.

Our specific-heat curves are in general qualitatively quite similar to those for the SMA potential:[7, 8] Na_8 in the SMA model has a broad peak, and Na_{20} a rather narrower peak with a small premelting feature on the low-temperature side. On the other hand, there are some differences with the TB specific-heat curves.[8] For instance, the specific heat of Na_8 has a somewhat narrower peak in the TB model than in the DB, KS, or SMA models. However, as noted above, the ground-state structure of Na_8 has a T_d symmetry in the TB model, but a D_{2d} symmetry in the DB, KS, and SMA models. Finally, Aguado *et. al.*, [14] using a model quite similar to the present DB-AI model, give *microcanonical* specific heats for Na_8 and Na_{20} , derived from a trajectory-based analysis, that appear to disagree qualitatively with the present DB and KS results (and with the SMA results.[7, 8]) Their curve for Na_8 has a single narrow peak with a width less than 30 K located around 110 K, while their curve for Na_{20} has two distinct peaks, each with a width less than 30 K and of similar height, located at about 110 K and 170 K. The precise reason for the differences between their results and the present results is unclear at present and requires further investigation. A re-evaluation of our own results in the microcanonical ensemble shows that the change of ensemble is insufficient to explain these differences, and we note that our DB ground-state geometries agree with theirs. Given the similarity between their DB model and ours, the discrepancies may be due simply to methodological differences: in the present work we have derived the specific-heat curves from a MH analysis, and have used longer sampling runs, checking that the specific-heat curves are reasonably stable against the addition of further data.

4 Conclusions

We have investigated the thermodynamics and melting of the small clusters Na_8 and Na_{20} using interionic potentials derived from several DFT models for the valence electrons. The data have been analyzed using a MH analysis, which is an efficient and reliable way of probing the melting transition. Of the various DFT models, the most accurate one considered here should be the KS-AI model. The other models involve substituting less accurate electron kinetic-energy functionals $T[\rho]$ (the DB approaches), or else soft, phenomenological pseudopotentials (the SP approaches) in place of *ab initio*

pseudopotentials, in each case with a view to accelerating the calculation and permitting better statistics. While there are qualitative similarities between the curves obtained from the various models, we also observe substantial shifts in temperatures of the main peaks and other features of the curves from model to model.

Concerning the choice of pseudopotential, while the SP pseudopotential is known to predict ground-state geometries and certain other properties well, as mentioned previously, it does not necessarily follow that energetic barriers and other important features of the potential-energy surface are well described. Given the substantial differences in the specific-heat curves obtained from the SP and AI pseudopotentials, it would therefore seem wise to prefer AI pseudopotentials. Note, however, that the soft pseudopotential used here is highly phenomenological: it lacks entirely a repulsive core, and deviates from the asymptotic value $-1/r$ for $r < \sim 3.7 a_0$, which is well outside the physical core of the Na^+ ion, $r < \sim 2.0 a_0$. It may be possible to construct a better soft pseudopotential that minimizes the difference with the specific-heat curve obtained from an AI pseudopotential and yet still yields a significantly cheaper calculation, thus permitting a very useful gain in statistics in thermodynamic simulations. We are currently investigating such possibilities.

As to the DB approach versus the full KS approach, we note that one important approximation in the DB approach in its present form is its difficulty in accounting for quantum shell effects accurately. The two DB forms for $T[\rho]$ considered here yield energies that vary smoothly with cluster size N according to a liquid-drop formula (as shown explicitly in Ref. [16] for the extended Thomas-Fermi functional), without showing the fluctuations in energy associated with quantum shell closures of the valence electrons. Further, while ground-state geometries and other properties of closed-shell systems can be predicted rather successfully by the DB approach [16, 22], it has trouble reproducing Jahn-Teller distortions in open-shell systems. Now, according to the Hohenberg-Kohn theorems, it should in principle be possible to find a DB functional $T[\rho]$ that fully incorporates such quantum shell effects in finite systems. It appears that if the DB methods are to yield reliable, quantitative information, then better electronic kinetic-energy functionals along these lines are required. Fortunately, significant progress is being made in this direction, and a number of researchers have already proposed DB kinetic-

energy functionals incorporating electronic shell effects approximately.

There is a special reason for paying careful attention to electronic shell effects in studies of melting that was mentioned earlier, related to the experiments of Haberland *et al.* [1]. The fact that prominent maxima in the melting point occur for sizes that are intermediate between geometric shell closures and electronic shell closures suggests that there is an important interplay between geometric effects and quantum shell effects. To understand this phenomenon more closely, we are currently considering Monte-Carlo sampling methods combined with various approximate KS schemes, with a view to extending the KS calculations presented in this work to larger sizes, within the range of the Haberland *et al.* data.

Acknowledgements

We gratefully acknowledge the support of the Indo-French Center for the Promotion of Advanced Research (New Delhi) / Centre Franco-Indien pour la Promotion de la Recherche Avancée under contract 1901-1. One of us (AMV) acknowledges the hospitality of the CEA, Grenoble, France. AMV is grateful to CSIR, New Delhi, India for their research fellowship. Thanks are also due to Matt Freigo and Stephen Johnson for an excellent FFT library.

References

- [1] M. Schmidt, R. Kusche, W. Kronmüller, B. von Issendorff, and H. Haberland, Phys. Rev. B **79**, 99 (1997); M. Schmidt *et al.*, Nature **393**, 238 (1998).
- [2] T. P. Martin, Phys. Rep. **273**, 199 (1996).
- [3] K. F. Peters, J. B. Cohen, and Y. W. Chung, Phys. Rev. B **57**, 13430 (1998).
- [4] D. J. Wells and R. S. Berry, Phys. Rev. Lett. **73**, 2875 (1994); T. L. Beck, D. M. Leitner, and R. S. Berry, J. Chem. Phys. **89**, 1681 (1993);

- T. L. Beck and R. S. Berry, *ibid.* **88**, 3910 (1993); H. L. Davis, J. Jellinek, and R. S. Berry, *ibid.* **86**, 6456 (1987); J. Jellinek, T. L. Beck, and R. S. Berry, J. Chem. Phys. **84**(5), 2783 (1986).
- [5] N. Ju and A. Bulgac, Phys. Rev. B **48**, 2721 (1993).
 - [6] Y. Li, E. Blaisten-Barojas, and D. A. Papaconstantopoulos, Phys. Rev. B **57**, 15519 (1998).
 - [7] F. Calvo and F. Spiegelmann, Phys. Rev. Lett. **82**, 2270 (1999).
 - [8] F. Calvo and F. Spiegelmann, J. Chem. Phys. **112**, 2888 (2000).
 - [9] R. Poteau, F. Spiegelmann, and P. Labastie, Z. Phys. D **30**, 57 (1994).
 - [10] R. Poteau and F. Spiegelmann, Phys. Rev. B **45**, 1878 (1992).
 - [11] J. Jellinek, S. Srinivas, and P. Fantucci, Chem. Phys. Lett. **288**, 705 (1998).
 - [12] Standard KS scales at least as $O(N^2)$.
 - [13] A. Vichare and D. G. Kanhere, J. Phys.: Condens. Matter **10**, 3309 (1998).
 - [14] A. Aguado, J. M. López, J. A. Alonso, and M. J. Stott, J. Chem. Phys. **111**, 6026 (1999).
 - [15] A. Aguado, J. M. López, J. A. Alonso, and M. J. Stott (to be published).
 - [16] P. Blaise, S. A. Blundell, and C. Guet, Phys. Rev. B **55**, 15856 (1997).
 - [17] A. M. Ferrenberg and R. H. Swendsen, Phys. Rev. Lett. **61**, 2635 (1988).
 - [18] P. Labastie and R. L. Whetton, Phys. Rev. Lett. **65**, 1567 (1990).
 - [19] M. C. Payne *et al.*, Rev. Mod. Phys. **64**, 1045 (1992).
 - [20] J. P. Perdew and A. Zunger, Phys. Rev. B **23**, 5048 (1981).
 - [21] S. K. Ghosh and L. C. Balbas, J. Chem. Phys. **83**, 5778 (1985).

- [22] D. Nehete, V. Shah, and D. G. Kanhere, Phys. Rev. B **53**, 2126 (1996); V. Shah, D. Nehete, and D. G. Kanhere, J. Phys.: Condens. Matter **6**, 10773 (1994); V. Shah and D. G. Kanhere, J. Phys.: Condens. Matter **8**, L253 (1996); V. Shah, D. G. Kanhere, C. Majumder, and G. P. Das, J. Phys.: Condens. Matter **9**, 2165 (1997).
- [23] G. B. Bachelet, D. R. Hamann, and M. Schlüter, Phys. Rev. B **26**, 4199 (1982).
- [24] R. Car and M. Parrinello, Phys. Rev. Lett. **55**, 685 (1985).
- [25] D. C. Payne, and J. D. Joannopoulos, Phys. Rev. Lett. **56**, 2656 (1986).
- [26] U. Röthlisberger and W. Andreoni, J. Chem. Phys. **94**, 8129 (1991).
- [27] Atomic units are used in the paper, unless otherwise explicitly stated.
- [28] F. Calvo and P. Labastie, Chem. Phys. Lett. **247**, 395 (1995).
- [29] P. Blaise and S. A. Blundell, submitted to Phys. Rev. (2000).
- [30] S. Nosé, Prog. Theor. Phys. Suppl. **103**, 1 (1991).
- [31] K. Hukushima and K. Nemoto, J. Phys. Soc. Japan **65**, 1604 (1995); U. H. E. Hansmann, Chem. Phys. Lett. **281**, 140 (1997).
- [32] V. Bonačič-Koutecký, P. Fantucci, and J. Koutecký, Phys. Rev. B **37**, 4369 (1988).

Figures

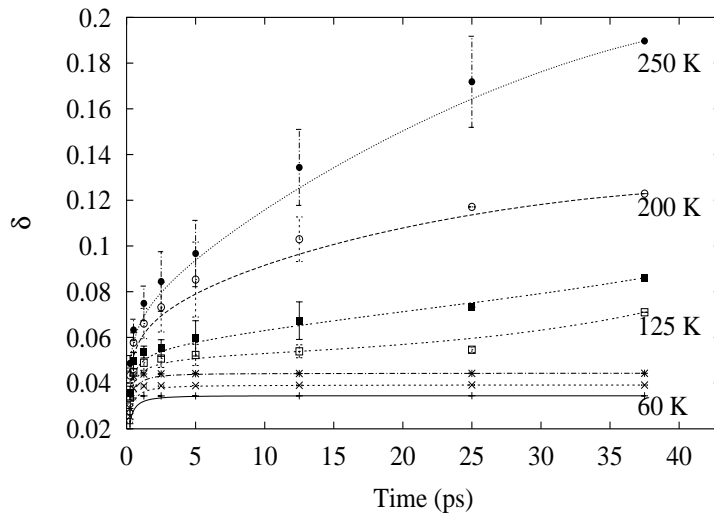


Figure 1: The rms bond-length fluctuation of Na_8 simulated using the KS-AI model as a function of time for various temperatures. Note that the tendency to converge is faster at low temperatures.

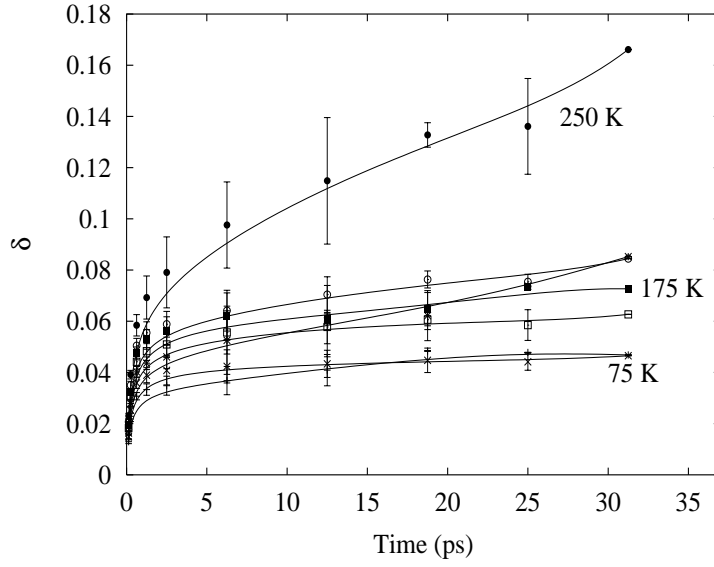


Figure 2: The rms bond-length fluctuation of Na_{20} simulated using the DB-AI model as a function of time for various temperatures. Note that the tendency to converge is faster at low temperatures.

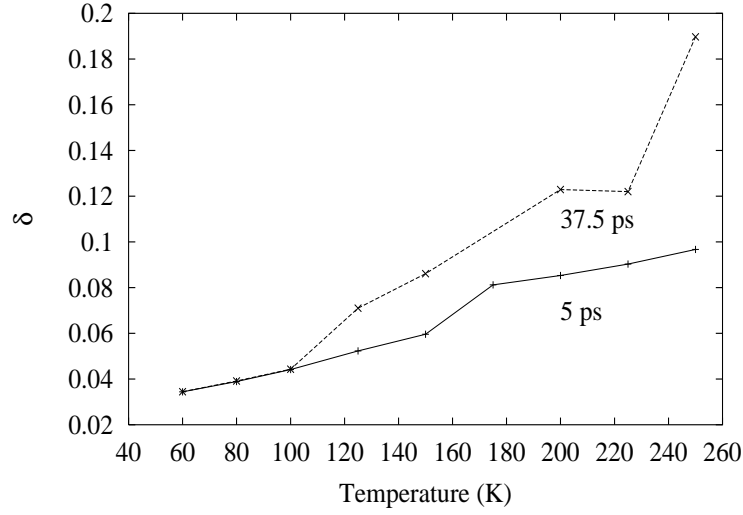


Figure 3: The rms bond-length fluctuation of Na_8 simulated using the KS-AI model as a function of temperature over 5 ps and 37.5 ps.

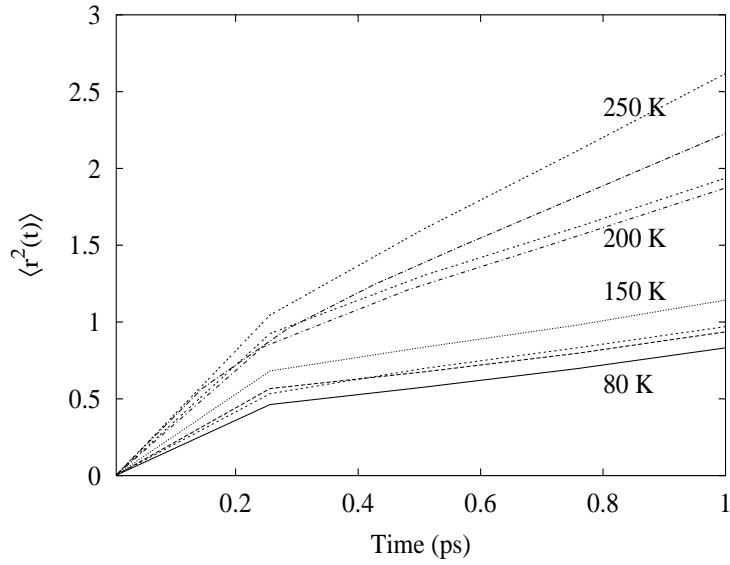


Figure 4: Mean square ionic displacements of Na_8 simulated using the KS-AI model at 1 ps time scale.

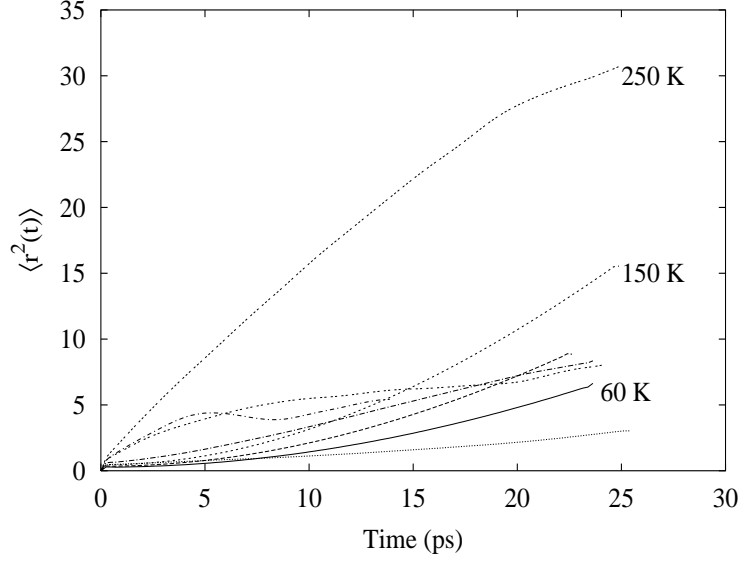


Figure 5: Mean square ionic displacements of Na_8 simulated using Kohn-Sham at 25 ps time scale.

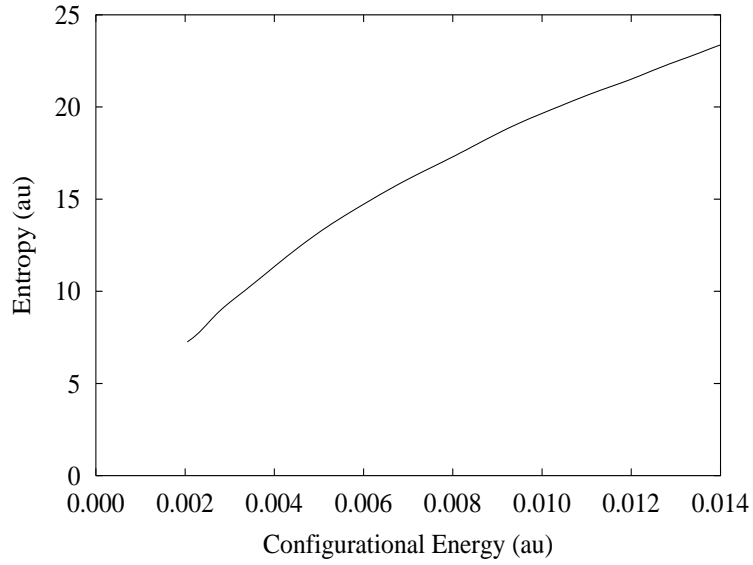


Figure 6: Ionic entropy of Na_8 for the KS-AI model extracted by the multiple histogram method.

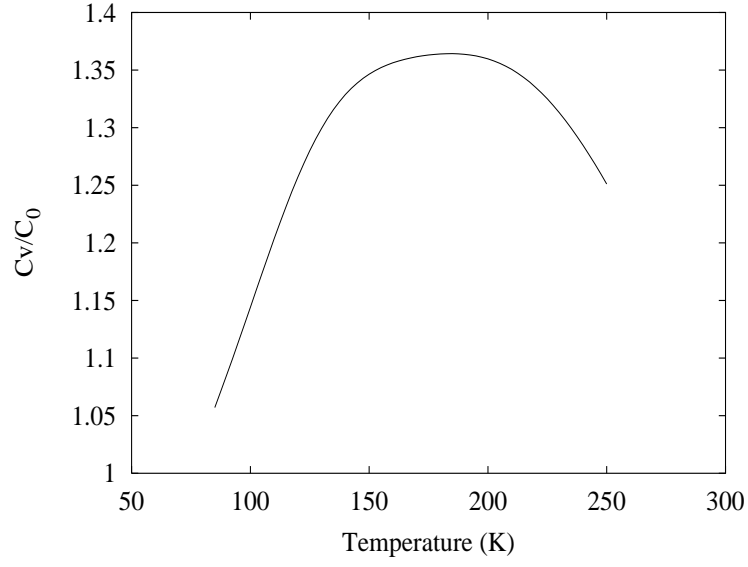


Figure 7: Canonical specific heat of Na_8 simulated using KS-AI.

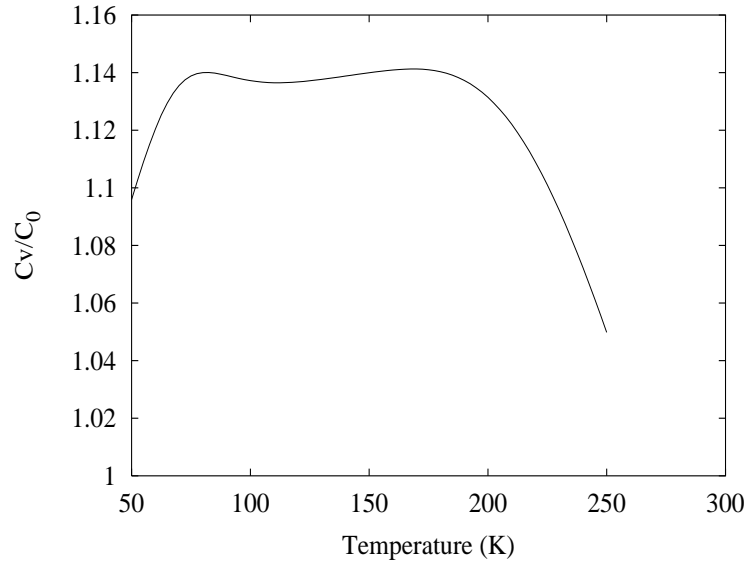


Figure 8: Canonical specific heat of Na_8 simulated using DB-AI.

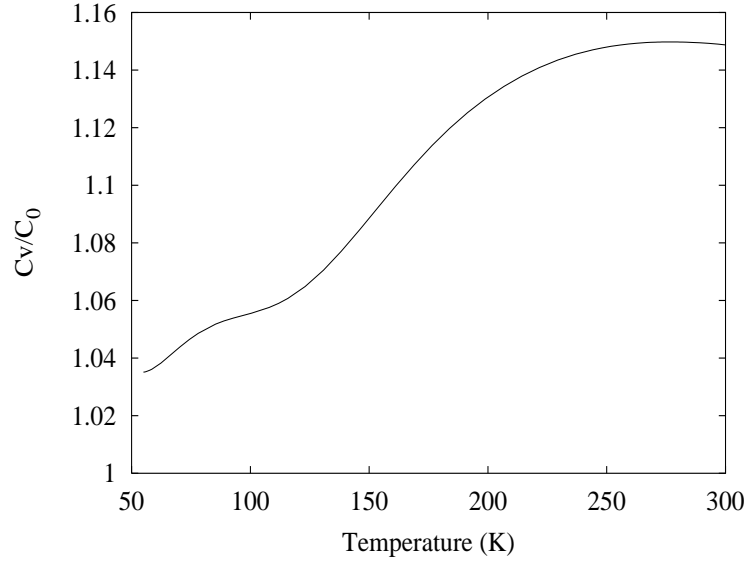


Figure 9: Canonical specific heat of Na_8 simulated using KS-SP.

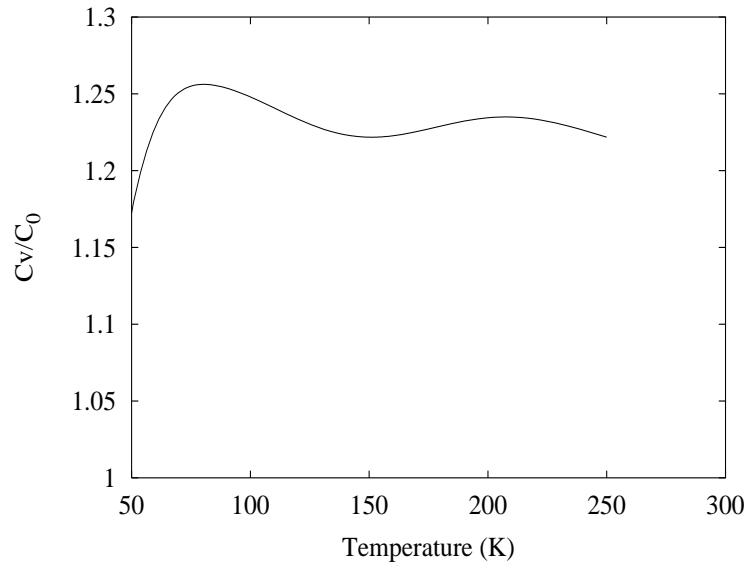


Figure 10: Canonical specific heat of Na_8 simulated using DB-SP.

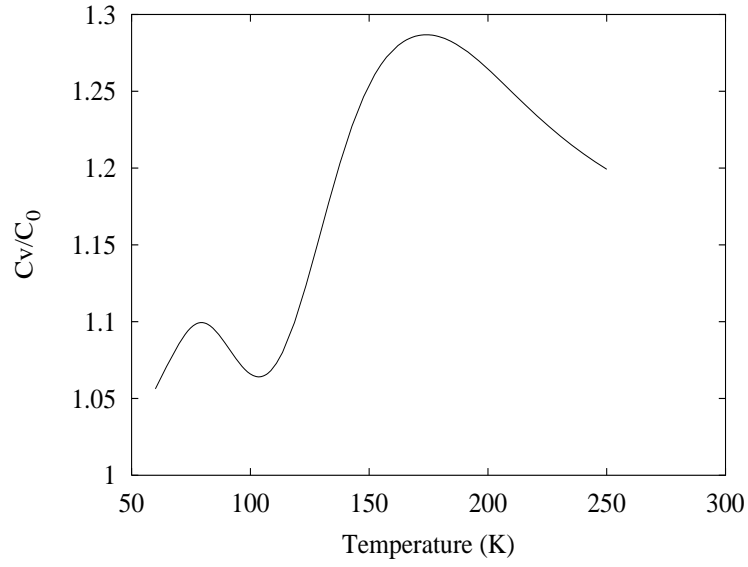


Figure 11: Canonical specific heat of Na_{20} simulated using KS-SP.

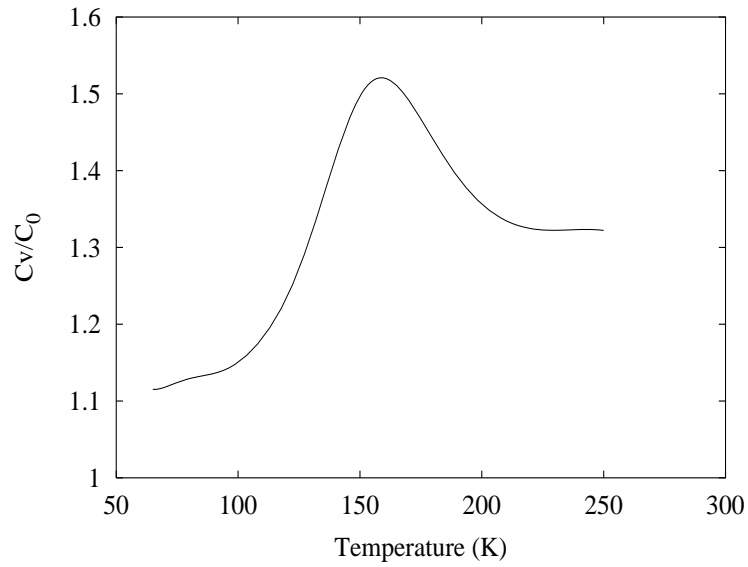


Figure 12: Canonical specific heat of Na_{20} simulated using DB-SP.

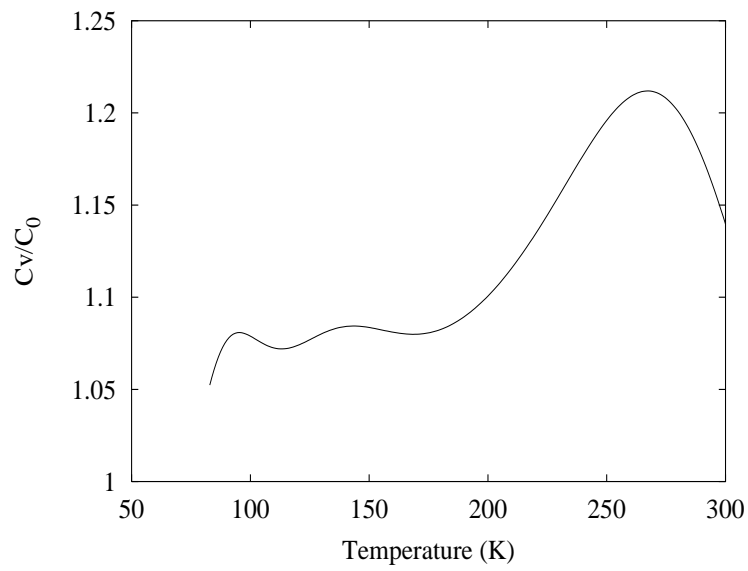


Figure 13: Canonical specific heat of Na_{20} simulated using DB-AI.